JCTC Journal of Chemical Theory and Computation

Direct Dynamics Implementation of the Least-Action Tunneling Transmission Coefficient. Application to the $CH_4/CD_3H/CD_4 + CF_3$ Abstraction Reactions

Rubén Meana-Pañeda,[†] Donald G. Truhlar,[‡] and Antonio Fernández-Ramos*,[†]

Department of Physical Chemistry and Center for Research in Biological Chemistry and Molecular Materials, University of Santiago de Compostela, 15782 Santiago de Compostela, Spain and Department of Chemistry and Supercomputing Institute, University of Minnesota, 207 Pleasant Street SE, Minneapolis, Minnesota 55455-0431

Received May 31, 2010

Abstract: We present two new direct dynamics algorithms for calculating transmission coefficients of polyatomic chemical reactions by the multidimensional least-action tunneling approximation. The new algorithms are called the interpolated least-action tunneling method based on one-dimensional interpolation (ILAT1D) and the double interpolated least-action tunneling (DILAT) method. The DILAT algorithm, which uses a one-dimensional spline under tension to interpolate both of the effective potentials along the nonadiabatic portions of tunneling paths and the imaginary action integrals as functions of tunneling energies, was designed for the calculation of multidimensional LAT transmission coefficients for very large polyatomic systems. The performance of this algorithm has been tested for the $CH_4/CD_3H/CD_4 + CF_3$ hydrogen abstraction reactions with encouraging results, i.e., when the fitting is performed using 13 points, the algorithm is about 30 times faster than the full calculation with deviations that are smaller than 5%. This makes direct dynamics least-action tunneling calculations practical for larger systems, higher levels of electron correlation, and/or larger basis sets.

1. Introduction

Hydrogen and proton transfer reactions are among the most prominent reactive processes in chemistry and biology.[1,2] These reactions are often dominated by quantum mechanical tunneling because the hydrogen atom, due to its small mass, can readily pass through classically forbidden regions of a potential energy surface (PES). Tunneling effects can be taken into account by rigorous quantum mechanical methods,[3−15] which are only applicable to systems with a small number of atoms, or by Wentzel−Kramers−Brillouin (WKB)-like semiclassical methods,[16−28] which can handle a large number of atoms. Among the semiclassical methods, variational transition-state theory with multidimensional tunneling corrections (VTST/MT)[29−42] is the best validated practical choice for the study of chemical reactions with several atoms because, on the one hand, it has proved to be very accurate when compared with quantum mechanical dynamics calculations[42,43] and, on the other hand, it needs only semiglobal information about the PES and in many cases is sensitive to the PES only near to the minimum-energy path.

The simplest case for VTST is when the transition-state dividing surface (which is the dynamical bottleneck for reaction) is located at a saddle point and the quantum effects on the reaction coordinate are negligible; in such a case, all the information required for the evaluation of thermal rate constants can be obtained from the reactants and the conventional transition state. In this case VTST/MT can be safely replaced by conventional transition-state theory.[44] Unfortunately, this is hardly ever the case for hydrogen transfer reactions, which, unless they have no barrier, are usually dominated by tunneling even up to temperatures well above room temperature.[40,42,43,45−49]

* Corresponding author. E-mail: qf.ramos@usc.es.
[†] University of Santiago de Compostela.
[‡] University of Minnesota.

10.1021/ct100285a
Published on Web 09/02/2010

Even when variational effects (i.e., effects due to the variational transition state not being located at a saddle point) are negligible, the incorporation of quantum effects in the VTST/MT treatment of generalized transition states requires more information about the PES than just reactants and transition-state properties. Quantum effects are incorporated differently for the reaction coordinate, which—for overbarrier processes—is the mode with an imaginary frequency at the saddle point and for the $F - 1$ normal modes of bound motion perpendicular to the reaction coordinate (where $F - 1$ equals $3N - 7$ for nonlinear transition states and $3N - 6$ for linear transition states, where N is the number of atoms, and the reaction coordinate is labeled as mode F). The thermal rate constant calculated by taking into account only the quantum effects on the coordinates in which motion is bound is called quasiclassical, and it is obtained by replacing the classical vibrational partition functions by quantum mechanical ones.[33,44,50] The quantum effects on the reaction coordinate are taken into account through a transmission coefficient[21,33,34,43,50−53] that multiplies the quasiclassical thermal rate constant. The evaluation of the transmission coefficient requires the selection of a tunneling path or paths.

As a zeroth approximation, one may assume that the tunneling path coincides with the minimum-energy path (MEP) (the union of the steepest-descent paths in isoinertial coordinates down from the saddle point to reactants and that down to products).[52,54,55] When zero-point effects are taken into account for bound motions transverse to the MEP, this assumption yields the zero-curvature tunneling (ZCT) approximation.[52] The signed distance from the saddle point along the MEP will be called the reaction coordinate, even though the dominant dynamical path may be offset from the MEP. The MEP is tangent to the imaginary frequency normal mode at the saddle point, so this definition coincides with defining the reaction coordinate in the vicinity of the saddle point as the distance along that mode.

It has been shown that the ZCT path, i.e., the MEP, is a poor choice as a tunneling path[42,56] since it does not take account of the MEP's curvature, which couples the reaction coordinate to the other vibrational modes. The curvature has the effect that the dominant tunneling path is on the concave side of the reaction path, and depending on the magnitude of the curvature, tunneling is better treated by the small-curvature tunneling (SCT) approximation[57−60] or by the large-curvature tunneling (LCT) approximation[23,37,41,59,61−65] for the cases of small and large couplings, respectively (for collinear atom−diatom reactions with very small curvature one could also use the Marcus−Coltrin approximation).[20] The path implied by the SCT approximation is not uniquely defined because the calculation is carried out in terms of an effective mass for tunneling along the MEP rather than using the true reduced mass along a tunneling path; the curvature-dependent effective mass is smaller than the true reduced mass to account for shortening of the tunneling path by corner cutting. The LCT approximation, in contrast, involves for every energy an explicit sequence of paths chosen as the straight lines that join equipotential points on the reactant and product sides of the vibrationally adiabatic potential curves along the MEP. Neither the SCT nor the LCT is variational; rather they represent limiting cases. However, the tunneling fluxes predicted by the SCT and LCT approximations roughly overlap for intermediate curvature, so they more or less cover the whole range of curvatures. It is reasonable to define a new tunneling probability that, at every tunneling energy, gives the larger of the SCT and LCT tunneling probabilities. This result is called the (microcanonically) optimized multidimensional tunneling probability (μOMT or, for short, OMT).[64] Note that the ZCT, SCT, LCT, and OMT tunneling approximations are all multidimensional in that they all include the important effect that the vibrational zero point energy (or, in the LCT and OMT approximations, also excited-state quantized vibrational energies) depends upon the distance along the reaction path or tunneling path; thus, the reaction coordinate is not separable in these approximations, and this mimics VTST in removing one of the major approximations of conventional transition-state theory. For this reason, it is most appropriate to apply these approximations in the context of VTST rather than conventional transition-state theory. The SCT, LCT, and OMT approximations include multidimensional effects not only in the vibrational energy requirements along the tunneling path but also in the choice of the tunneling path.

Very recently[28] we have generalized to polyatomic reactions the least-action tunneling (LAT) path, which was initially developed by Garrett and Truhlar for atom−diatom reactions.[22] In this approximation, one considers, for each tunneling energy and final vibrational state, a sequence of paths parametrized by a unique parameter. These paths are all located at or between the MEP and LCT paths. At every tunneling energy, the path is variationally optimized within this sequence by choosing it as the path with the largest tunneling probability. For this reason, in principle, the LAT transmission coefficients should be more accurate than those obtained by the μOMT approximation.

The current version of the LAT method for ground-state transmission coefficients (which are used to calculate thermally averaged rate constants)[41] may be called the least-action ground-state tunneling method, version 4, (LAG4) because we always base the transmission coefficients for thermal reactions on a ground-state transmission coefficient (computed in the exoergic direction) and because the LCT-like portions of the calculation are based on version 4 of the LCT method.[65] (Note that, although the reactant is in the ground state for the prototype tunneling process on which the calculation of the thermally averaged rate is based, a range of vibrational states is populated in the product of the tunneling event, if the energy is high enough to populate dynamically coupled states in the product valley, and tunneling for excited-state reactants is approximated in terms of the ground-state tunneling probabilities and the quantized threshold energies at the variational transition state.) The present article is concerned with the calculation of LAG4 transmission coefficients, and we will simply abbreviate them as LAT. Similarly we use LCT as shorthand for LCG4.

The LCT, μOMT, and LAT transmission coefficients are more computationally intensive than the SCT one because, whereas the SCT transmission coefficient can be obtained from a very limited knowledge of the PES, i.e., from

information calculated along the MEP (including its curvature and local force constants for motion transverse to the MEP), the calculation of the other transmission coefficient approximations requires information not only along the MEP but also in the wide region on the concave side of the MEP. This region is called the reaction swath,[66,67] and it is the region through which LCT and LAT tunneling paths pass. The LCT, μOMT, and LAT transmission coefficients involve the calculation of a potentially large number of points of the PES in the reaction swath. The development of faster computers and more accurate density functionals has made it possible in many cases to evaluate the energy reasonably accurately at those geometries by direct dynamics, which allows "the calculation of rates or other observables directly from electronic structure information without intermediacy of fitting the electronic energies in the form of a potential energy surface".[68] Direct dynamics together with VTST/MT is a powerful combination that, for instance, is being widely used in the evaluation of thermal rate constants and kinetic isotope effects (KIEs) of many enzymatic reactions.[69]

However, the calculation of LCT and LAT transmission coefficients by direct dynamics is still computationally very demanding if one uses the original algorithms. For that reason we developed an algorithm (called ILCT2D) based on a two-dimensional spline-under-tension,[70] to evaluate LCT tunneling probabilities with a reduction in the computer time by a factor of about 30.[71] The error with respect to the full calculation is less than 1%. It is the objective of the present work to present an analogous efficient algorithm based on spline-under-tension interpolations for calculation of LAT transmission coefficients using direct dynamics, and we will present two such algorithms. To show the performance of the new algorithms, we have chosen the following set of hydrogen abstraction reactions:

$$CH_4 + CF_3 \rightarrow CH_3 + HCF_3 \quad \text{(R1)}$$

$$CD_3H + CF_3 \rightarrow CD_3 + HCF_3 \quad \text{(R2)}$$

$$CD_3H + CF_3 \rightarrow CD_2H + DCF_3 \quad \text{(R3)}$$

$$CD_4 + CF_3 \rightarrow CD_3 + DCF_3 \quad \text{(R4)}$$

which we have previously studied using the SCT, LCT (with the ILCT2D algorithm), and μOMT approximations for tunneling.[71] The calculated thermal rate constants were in good agreement with experimental data. However, the calculated KIEs were too low, particularly those for the ratio R2/R3. In this paper, in addition to developing a more efficient algorithm for LAT calculations, we use it to apply the LAT approximation to these reactions to see if this method improves the previous results.

Section 2 presents a general description of the evaluation of tunneling transmission coefficients and presents the new interpolation schemes used for efficient direct dynamics calculations of LAT transmission coefficients. Section 3 describes the performance of those interpolation schemes for reactions R1−R4. Section 4 has concluding remarks.

2. Methodology

The VTST/MT thermal rate constant[37,41] can be written as the quasiclassical canonical variational theory (CVT) rate constant k^{CVT} multiplied by the tunneling transmission coefficient, $\kappa^{CVT/X}$, i.e.,

$$k^{CVT/X}(T) = \kappa^{CVT/X}(T)k^{CVT}(T) \quad (1)$$

where X stands for the ZCT,[52] SCT,[60] LCT,[22,64,65] μOMT,[64] or LAT[22,28] approximations for tunneling. In general $\kappa^{CVT/X}$ is equal to a so-called CAG factor (called $\kappa^{CVT/CAG}$ and almost always very close, within about 15%, to unity) times a more universal transmission coefficient called κ^X. Since the CAG factor is explained in detail elsewhere,[21,37,41] we concentrate here on κ^X.

The ZCT approximation assumes that the reaction coordinate is adiabatically separated from the $F - 1$ other degrees of freedom and that all the excited-state vibrationally adiabatic potentials that significantly contribute to tunneling have the same shape as the ground-state vibrationally adiabatic potential $V_a^G(s)$, which is given by

$$V_a^G(s) = V_{MEP}(s) + \varepsilon_{vib}^G(s) \quad (2)$$

where s is the reaction coordinate mentioned in Section 1 (it measures progress along the isoinertial MEP, being negative on the reactants side, zero at the saddle point, and positive on the products side, where the isoinertial coordinates are scaled to a reduced mass of μ); $V_{MEP}(s)$ is the potential along the MEP; and $\varepsilon_{vib}^G(s)$ is the local zero-point vibrational energy. The other tunneling approximations also involve the $V_a^G(s)$ but in more complicated ways.

The lowest energy possible to have tunneling is the energy of the reactant zero-point level when the reaction is written in the exoergic direction; this is called E_0. The transmission coefficient is given by

$$\kappa^X(T) = \beta \exp(\beta V_a^{AG}) \int_{E_0}^{\infty} dE P^X(E) \exp(-\beta E) \quad (3)$$

where $\beta = (k_B T)^{-1}$, k_B is the Boltzmann constant, and T is the temperature; V_a^{AG} is the maximum of the ground-state vibrationally adiabatic potential; and $P^X(E)$ is the ground-state semiclassical probability at energy E, which is approximated in the ZCT and SCT approximations as

$$P^X(E) = \begin{cases} 0, & E < E_0 \\ \{1 + \exp[2\theta(E)]\}^{-1}, & E_0 \le E \le V_a^{AG} \\ 1 - P^X(2V_a^{AG} - E), & V_a^{AG} \le E \le 2V_a^{AG} - E_0 \\ 1, & 2V_a^{AG} - E_0 < E \end{cases} \quad (4)$$

where $\theta(E)$ is the imaginary part of the action integral. When X = μOMT, the tunneling probabilities are obtained as[64]

$$P^{\mu OMT} = \max_E \begin{cases} P^{SCT}(E) \\ P^{LCT}(E) \end{cases} \quad (5)$$

where P^{LCT} is obtained from a more complicated expression than P^{SCT}.

In the LCT and LAT approximations, one must sum over tunneling probabilities from the ground state of the reactants to all accessible diabatic vibrational states of the product. In many cases, only the ground-state-to-ground-state process needs to be considered. Even when the excited states of the product must be considered, it is sufficient to consider the ground-state-to-ground-state case to explain the new algorithms being introduced here, and so we limit our consideration to the ground-state-to-ground-state case. (We previously found[71] that tunneling into excited vibrational states does not make a large contribution for the reactions under consideration here.)

For a given tunneling path, the imaginary part of the action integral is given by

$$\theta(E) = \hbar^{-1} \int_{\xi_0}^{\xi_1} \mathrm{Im}\, p(\xi) d\xi \tag{6}$$

where ξ is a progress variable along the tunneling path; ξ_0 and ξ_1 mark the beginning and end of the tunneling path, respectively; and Im $p(\xi)$ is the imaginary part of the momentum in the tunneling direction, which is written as

$$p(\xi) = \{2\mu_{\mathrm{eff}}(\xi)[E - V_{\mathrm{eff}}(\xi)]\}^{1/2} \tag{7}$$

where $\mu_{\mathrm{eff}}(\xi)$ and $V_{\mathrm{eff}}(\xi)$ are respectively the effective reduced mass and the effective potential along the tunneling path. The calculation of the transmission coefficient of eq 3 requires the evaluation of tunneling probabilities at several energies, and these depend on the tunneling paths. For X = ZCT the tunneling path coincides with the MEP, and therefore the progress variable along the path is s, and the effective potential is given by the ground-state vibrationally adiabatic potential given by eq 2. The effective mass $\mu_{\mathrm{eff}}(s) = \mu$. Therefore, in the ZCT approximation the action integral, at every tunneling energy, is given by

$$\theta(E) = \hbar^{-1} \int_{\tilde{s}_0}^{\tilde{s}_1} ds\{2\mu(V_{\mathrm{a}}^{\mathrm{G}}(s) - E)\}^{1/2} \tag{8}$$

where $\tilde{s}_0$ and $\tilde{s}_1$ are the classical turning points in the reactant and product valleys, respectively. Both turning points obey the resonance condition:

$$V_{\mathrm{a}}^{\mathrm{G}}(\tilde{s}_0) = V_{\mathrm{a}}^{\mathrm{G}}(\tilde{s}_1) = E \tag{9}$$

and therefore it is equivalent to write $\theta(E)$ or $\theta(\tilde{s}_0)$ in eq 8.

The coupling between the reaction coordinate and the $F - 1$ other modes produces an internal centrifugal effect that shortens the dominant tunneling path at a given energy by displacing it toward the concave side of the MEP. The SCT approximation incorporates this effect in the effective mass for tunneling without an explicit evaluation of the tunneling path. The SCT action integral is given by

$$\theta(E) = \hbar^{-1} \int_{\tilde{s}_0}^{\tilde{s}_1} ds\{2\mu_{\mathrm{eff}}(s)(V_{\mathrm{a}}^{\mathrm{G}}(s) - E)\}^{1/2} \tag{10}$$

It should be noticed that now the effective mass depends on the progress along the MEP and that $\mu_{\mathrm{eff}} \leq \mu$. For this reason the SCT transmission coefficient is always larger or equal to the ZCT transmission coefficient.

To evaluate the LAT tunneling probability, one must calculate the action integrals of a family of tunneling paths that depend on a parameter α. These paths correspond to the MEP when $\alpha = 0$ and to the LCT path, which is a straight path, for $\alpha = 1$. Let $\xi_{\mathrm{P}}(0)$ be the length of the tunneling path along the MEP from $\tilde{s}_0$ to $\tilde{s}_1$ (this is equal to $\tilde{s}_1 - \tilde{s}_0$), and let $\xi_{\mathrm{P}}(1)$ be the length of the straight-line path, which is shorter. Then, the geometry of a point on the path with parameter α is given by

$$\mathbf{x}[\alpha, \xi(\alpha), \tilde{s}_0] = (1 - \alpha)\mathbf{x}[0, \xi(0), \tilde{s}_0] + \alpha\mathbf{x}[1, \xi(1), \tilde{s}_0] \tag{11}$$

where $\mathbf{x}[0, \xi(0), \tilde{s}_0]$ and $\mathbf{x}[1, \xi(1), \tilde{s}_0]$ are respectively geometries on the MEP and on the straight path; thus $\xi(1)$ is equal to $\xi(0)$ times the ratio of $\xi_{\mathrm{P}}(1)$ to $\xi_{\mathrm{P}}(0)$. Consequently, the progress variable ξ depends on the value of the α parameter, and $\xi(1)$ is less than or equal to $\xi(\alpha)$, which is less than or equal to $\xi(0)$. The probabilities along the series of paths of eq 11 may involve regions of the PES that are vibrationally nonadiabatic (see refs. 28 and 41 for details), so in general the action integral is split into three terms:

$$\theta(\alpha, E) = \theta_{\mathrm{I}}(\alpha, E) + \theta_{\mathrm{II}}(\alpha, E) + \theta_{\mathrm{III}}(\alpha, E) \tag{12}$$

The action integrals $\theta_i(\alpha, E)$, with i = I and III, correspond to the adiabatic regions on the reactants (i = I) and products (i = III) side, respectively, and they are given by the following expressions:

$$\theta_{\mathrm{I}}(\alpha, E) = \hbar^{-1} \int_0^{\xi_{\mathrm{I}}(\alpha)} d\xi(\alpha)\{V_{\mathrm{a}}^{\mathrm{G}}[s_{\mathrm{I}}(0, \xi(0)); \tilde{s}_0)] - V_{\mathrm{a}}^{\mathrm{G}}(\tilde{s}_0)\}^{1/2} \cos\chi_0 \tag{13}$$

$$\theta_{\mathrm{III}}(\alpha, E) = \hbar^{-1} \int_{\xi_{\mathrm{III}}(\alpha)}^{\xi_{\mathrm{P}}(\alpha)} d\xi(\alpha)\{V_{\mathrm{a}}^{\mathrm{G}}[s_{\mathrm{III}}(0, \xi(0)); \tilde{s}_0)] - V_{\mathrm{a}}^{\mathrm{G}}(\tilde{s}_0)\}^{1/2} \cos\chi_1 \tag{14}$$

The total length of the path is $\xi_{\mathrm{P}}(\alpha)$; and the values $\xi_{\mathrm{i}}(\alpha)$ i = I and III indicate boundaries of the adiabatic region. Each of the $s_i(0, \xi(0))$, i = I and III values needed for the evaluation of the vibrationally adiabatic potentials $V_{\mathrm{a}}^{\mathrm{G}}[s_i(0, \xi(0)); \tilde{s}_0)]$, is obtained in such a way that the vector defined by the geometry $\mathbf{x}[\alpha, \xi(\alpha), \tilde{s}_0]$ and the reaction path geometry $\mathbf{x}[0, \xi(0), \tilde{s}_0]$ is perpendicular to the derivative of $\mathbf{x}[0, \xi(0), \tilde{s}_0]$ with respect to s at that s value, i.e.,

$$\{\mathbf{x}[\alpha, \xi(\alpha), \tilde{s}_0] - \mathbf{x}[0, \xi(0), \tilde{s}_0]\} \cdot \frac{\mathrm{d}\mathbf{x}[0, \xi(0), \tilde{s}_0]}{\mathrm{d}s} = 0 \tag{15}$$

The angles between the gradient and tangent vector to the path at $\tilde{s}_0$ and $\tilde{s}_1$ are χ_0 and χ_1, respectively. If the entire path is adiabatic (i.e., if there is no region II), then there will be overlap between regions I and III in the interval $\xi_{\mathrm{III}}(\alpha) \leq \xi(\alpha) \leq \xi_{\mathrm{I}}(\alpha)$, and the vibrationally adiabatic potential in that region is taken to be

$$\min\{V_{\mathrm{a}}^{\mathrm{G}}[s_{\mathrm{I}}(0, \xi(0)); \tilde{s}_0)], V_{\mathrm{a}}^{\mathrm{G}}[s_{\mathrm{III}}(0, \xi(0)); \tilde{s}_0)]\} \tag{16}$$

The action integral through the nonadiabatic region is given by

$$\theta_{II}(\alpha, E) = \hbar^{-1} \int_{\xi_I(\alpha)}^{\xi_{III}(\alpha)} d\xi(\alpha) \{ V_{eff}^{II}(\alpha, \xi(\alpha), \tilde{s}_0) - V_a^G(\tilde{s}_0) \}^{1/2} \quad (17)$$

The effective potential $V_{eff}^{II}(\alpha, \xi(\alpha), \tilde{s}_0)$ is obtained from

$$V_{eff}^{II}(\alpha, \xi(\alpha), \tilde{s}_0) = V\{\mathbf{x}[\alpha, \xi(\alpha), \tilde{s}_0]\} + V_{corr}^{I}(\alpha, \xi_I(\alpha), \tilde{s}_0) + V_{anh}^{I}(\alpha, \tilde{s}_0) + \frac{\xi(\alpha) - \xi_I(\alpha)}{\xi_{III}(\alpha) - \xi_I(\alpha)} [V_{corr}^{III}(\alpha, \xi_{III}(\alpha), \tilde{s}_0) - V_{corr}^{I}(\alpha, \xi_I(\alpha), \tilde{s}_0) + V_{anh}^{III}(\alpha, \tilde{s}_0) - V_{anh}^{I}(\alpha, \tilde{s}_0)] \quad (18)$$

In this expression the potentials $V_{corr}^{i}(\alpha, \xi_i(\alpha), \tilde{s}_0)$, $i = \mathrm{I}$ and III correct for the zero-point energy in the modes that still behave adiabatically. The potentials $V_{anh}^{i}(\alpha, \tilde{s}_0)$ incorporate anharmonic nonquadratic corrections to the effective potential in the same way as in eq 5 of the LCT method.[65] The geometries $\mathbf{x}[\alpha, \xi(\alpha), \tilde{s}_0]$, needed for the evaluation of the classical potential $V\{\mathbf{x}[\alpha, \xi(\alpha), \tilde{s}_0]\}$, are obtained from the straight path joining the geometries $\mathbf{x}[\alpha, \xi_I(\alpha), \tilde{s}_0]$ and $\mathbf{x}[\alpha, \xi_{III}(\alpha), \tilde{s}_0]$, i.e.,

$$\mathbf{x}[\alpha, \xi(\alpha), \tilde{s}_0] = \mathbf{x}[\alpha, \xi_I(\alpha), \tilde{s}_0] + \frac{\xi(\alpha) - \xi_I(\alpha)}{\xi_{III}(\alpha) - \xi_I(\alpha)} (\mathbf{x}[\alpha, \xi_{III}(\alpha), \tilde{s}_0] - \mathbf{x}[\alpha, \xi_I(\alpha), \tilde{s}_0]) \quad (19)$$

We note that the LCT expressions are obtained for the effective potential of eq 18 and the action integrals of eqs 12−14 and 17 when $\alpha = 1$.

Converged probabilities at every tunneling energy are obtained by the numerical integration of eqs 13, 14, and 17 at N points along the path; for the present work we set $N = 180$. If there is a nonadiabatic region, then N_I of those N points belong to region I, N_{II} are in region II, and N_{III} are in region III. The potential in regions I or III is obtained from the vibrationally adiabatic potential along the MEP. However, the effective potential at the geometries obtained from eq 19 requires single-point calculations of the potential energy at points $\xi_i(\alpha)$, $i = 1, ..., N_{II}$, where $\xi_1(\alpha) = \xi_I(\alpha)$ and $\xi_{N_{II}}(\alpha) = \xi_{III}(\alpha)$. We found that the evaluation of the LCT transmission coefficients by the interpolated large-curvature tunneling algorithm based on one-dimensional interpolation (ILCT1D)[72] of these potential energies almost perfectly reproduces the specifically calculated potentials $V\{\mathbf{x}[1, \xi(1), \tilde{s}_0]\}$ when the N_{II} points are replaced by $N_S = 9$ equally spaced points, which are interpolated by a one-dimensional spline-under-tension.[73,74] If, at a given tunneling energy, $N_{II} < 9$, then no interpolation is carried out along the nonadiabatic region of the tunneling path. Similarly, the above procedure can be used to obtain the LAT transmission coefficients; the only difference being that now N_S points are used to evaluate the α-dependent effective potential of eq 18. We call this algorithm the interpolated least-action tunneling method based on one-dimensional interpolation (ILAT1D).

The calculation of transmission coefficients by the full-LAT method (without any interpolation) using direct dynamics requires a large amount of computer time, so we tested the performance of the ILAT1D algorithm by using analytical PESs. We used the same analytical PESs as for the testing of the ILCT1D method and found that the mean unsigned percentage error (MUPE) of the ILAT1D algorithm with respect to a full LAT calculations (as a reference) is smaller than 0.20% in the interval from $T = 200-400$ K (see Supporting Information for further details of these tests). Therefore, we believe that the transmission coefficients obtained by the ILAT1D algorithm can safely replace full LAT calculations without loss of accuracy. Hereafter, we use the ILAT1D algorithm as a reference in the development of more approximate algorithms, as discussed below.

The ILAT1D algorithm is still very expensive in computer time, since the value, $\tilde{\alpha}$, of α that minimizes the action of eq 12 is obtained by a golden section search[75] at every tunneling energy. Therefore, we developed another, even more efficient algorithm that further reduces the number of tunneling energies at which the least-action integral, $\theta(\tilde{\alpha}, E)$, has to be explicitly computed. The method is described next.

In the ILAT1D algorithm the least-action integral is evaluated at tunneling energies E_i, $i = 1, ..., M$, with E_1 being the lowest energy at which it is possible to locate the classical turning points that determine the straight path and M being the number of tunneling energies (all below the maximum of the vibrationally adiabatic potential) at which the tunneling probabilities are calculated. In general, one has $40 \leq M \leq 80$. The tunneling energies that are computationally most demanding are those for which there is a nonadiabatic region for some of the possible tunneling paths. It should be noticed that the absence of nonadiabatic region at a given tunneling energy along the LCT path means also the absence of nonadiabatic regions at any of the α-dependent paths at that tunneling energy and makes the LAT and LCT probabilities coincide. The potential in the adiabatic region is readily available, because it can be obtained from information along the MEP. Therefore the effort in developing the more efficient algorithm is focused on the E_i, $i = 1, ..., M_{II}$ tunneling energies with nonadiabatic regions along the straight path, where $E_{i=M_{II}}$ is the highest tunneling energy for which there is a nonadiabatic region along the LCT path. It is possible to reduce computer time by explicitly evaluating the least-action integral at M_S tunneling energies instead of at M_{II} tunneling energies. The remaining least-action integrals are obtained implicitly by interpolation with a one-dimensional spline-under-tension. The M_S tunneling energies are chosen in such a way that E_1 and $E_{M_{II}}$ are the first and last energies of the fit, respectively, and the remaining $M_S - 2$ energies are taken as equally spaced between those two values. (We also considered interpolating $\tilde{\alpha}$ instead of $\theta(\tilde{\alpha}, E)$, but we found, as shown in Section 3, that the latter is a much better choice because $\theta(\tilde{\alpha}, E)$ changes smoothly with the tunneling energy.) In summary, the new algorithm uses one-dimensional interpolation for both the tunneling paths and the optimized action integrals, and therefore we call the method the double interpolated least-action tunneling (DILAT) method.

The remaining steps are explained fully in previous discussions of the LCT and LAT methods[28,41,59,76] and so are only briefly summarized here. The least-action integrals obtained at every tunneling energy are used to compute tunneling amplitudes defined by

$$T_{\mathrm{tun}}^{\mathrm{LAT}}(\tilde{\alpha}, \tilde{s}_0) = T_{\mathrm{tun}}^{\mathrm{LAT}}(\tilde{\alpha}, \tilde{s}_1) = \exp[-\theta(\tilde{\alpha}, \tilde{s}_0)] \quad (20)$$

The LAT primitive probability at every tunneling energy, using either the ILAT1D or DILAT algorithm, is obtained from the tunneling amplitude of eq 20 plus the contribution due to the vibrational motion perpendicular to the reaction coordinate along the incoming and outgoing trajectories. The LAT primitive probability is then uniformized such that it goes to half of the maximum of the ground-state vibrationally adiabatic potential. The resulting LAT tunneling probabilities are also used for the calculation of the nonclassical over-the-barrier tunneling probabilities, as in eq 4.

Note that the μOMT transmission coefficient is always greater than or equal to both the SCT and LCT ones, and the LAT transmission coefficient is always greater than or equal to the LCT one. However, the LAT transmission coefficient can be either greater or smaller than the SCT one, because the LAT paths lie between the MEP and LCT paths, but the LAT method does not incorporate the small-curvature limit explicitly.

A full calculation of the LAT transmission coefficients scales as $M \times N \times L$, since for each of the M tunneling energies, we need to perform L iterations to obtain a converged least-action integral on tunneling paths obtained with N single-point calculations. Typical values for these parameters are $M = 60$, $N = 180$, and $L = 25$, which involves approximately 3×10^5 single-point energy calculations. Many of those points fall in the adiabatic regions, so they can be readily calculated from the information available along the MEP, and only the evaluation of the effective potential of nonadiabatic region II requires additional direct dynamics electronic structure calculations. The number of points in the nonadiabatic region in the full calculation would be $M_{\mathrm{II}} \times \bar{N}_{\mathrm{II}} \times L$, where $\bar{N}_{\mathrm{II}}$ is the average of nonadiabatic points at every tunneling energy. The size of the nonadiabatic region depends on the PES, but reasonable numbers for M_{II} and $\bar{N}_{\mathrm{II}}$ are 40 and 50, respectively, and therefore the number of single-point calculations in the nonadiabatic region is approximately 5×10^4. The ILAT1D algorithm reduces the number of single-point calculations to $M_{\mathrm{II}} \times N_S \times L$ such that it requires approximately 9000 single-point calculations in the nonadiabatic region. The DILAT algorithm reduces further the number of single-point calculations by the ratio M_{II}/M_S.

The ILAT1D and the DILAT algorithms for the calculation of LAT transmission coefficients using direct dynamics have been implemented in a development version of POLYRATE,[77] and we plan that they will be made available in an upcoming new release version of the program.

3. Applications

The electronic structure calculations needed for the evaluation of LAT transmission coefficients for reactions R1−R4 using the ILAT1D and DILAT algorithms were performed with the MPWB1K[78] density functional using the 6-31+G(d,p) basis set.[79] The details of the electronic structure calculations can be found in ref 71. The previous calculations showed that the maximum of the vibrationally adiabatic potential occurs at the saddle point, that is, $V_{\mathrm{a}}^{\mathrm{AG}} = V_{\mathrm{a}}^{\ddagger \mathrm{G}}$, and that there are no variational effects in the interval of temperatures between 200 and 700 K, so the variational dividing surface is located at the conventional transition state. Besides, $\kappa^{\mathrm{CVT/X}}$ of eq 1 equals κ^{X} because $\kappa^{\mathrm{CVT/CAG}} = 1$.

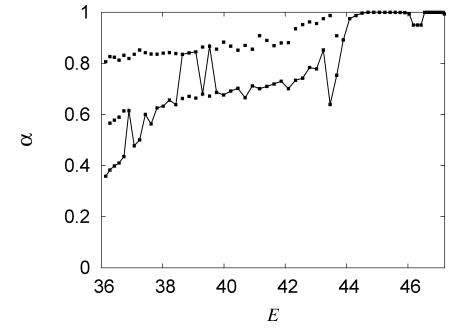

Figure 1. Plot of the α parameter versus the tunneling energy (E, in kcal·mol^{-1}) relative to the reactants at their equilibrium separation without zero-point energy. The dots correspond to the values of α at which there are local minima of the imaginary action integral at all of the calculated tunneling energies. The solid line joins the global minimum of the α parameter, $\tilde{\alpha}$, at every tunneling energy.

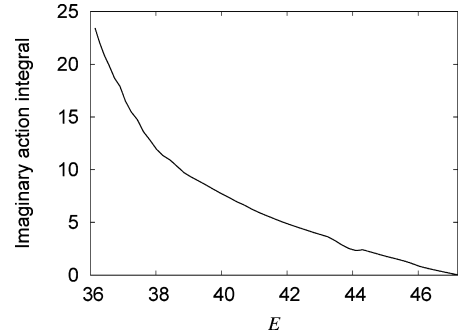

Figure 2. The solid line shows the variation of the imaginary action integral, $\theta(\tilde{\alpha}, E)$, of eq 12 with the tunneling energy (in kcal·mol^{-1}).

Figure 1 shows that the values of $\tilde{\alpha}$ at different tunneling energies may change abruptly, which makes a fit of $\tilde{\alpha}$ as a function of tunneling energy quite difficult and inaccurate, so instead we chose to interpolate the action integrals corresponding to $\tilde{\alpha}$. It is noteworthy that there are several tunneling energies with two or even three local minima for the imaginary action integral. However, even in this difficult case, an interpolation of the least-action integral as a function of tunneling energy is easier to perform than an interpolation of $\tilde{\alpha}$ due to the smooth behavior of $\theta(\tilde{\alpha}, E)$, as shown in Figure 2.

Table 1 lists the number of single-point calculations needed to evaluate the effective potential of eq 18 for R1 for the calculation of the LAT transmission coefficients with the ILAT1D and DILAT algorithms (the number of points for R2−R4 is similar to R1 and is not shown in the table). We use as reference calculations those obtained by the ILAT1D algorithm. The ILAT1D algorithm allows one to obtain LAT transmission coefficients 7.5 times faster than the full LAT calculation. In this case the DILAT algorithm is 50 and 20

Table 1. Number of Single-Point Calculations (NSP) in the Nonadiabatic Region Needed for the Calculation of the LAT Transmission Coefficients with Selected Values of M_S for Reaction R1

level	M_S	NSP
full	43	137 895
ILAT1D	43	18 564
DILAT	7	2809
	9	3699
	13	5165
	17	7264

Table 2. MUPEs for Reactions R1−R4 of the LAT Transmission Coefficients Obtained by DILAT for Different Numbers of Fitting Points, M_S, When Compared with ILAT1D Reference Values

	MUPE			
M_S	R1	R2	R3	R4
		$T = 250$ K		
5	16.56	17.76	1.70	18.11
7	7.88	7.12	2.08	0.61
9	9.54	11.32	6.17	1.33
11	9.00	12.12	0.54	3.58
13	0.51	1.28	3.06	2.27
15	1.74	2.59	0.77	5.25
17	0.51	2.15	0.02	4.86
19	3.68	5.10	0.63	5.83
		$T = 300$ K		
5	13.06	14.12	1.19	4.62
7	6.06	5.20	0.27	1.04
9	9.85	9.90	2.93	1.31
11	8.79	9.31	0.29	0.69
13	1.30	1.67	1.39	0.40
15	1.39	2.13	0.36	1.21
17	0.61	1.79	0.01	0.97
19	4.02	4.28	0.36	1.56

times faster than the full calculation for $M_S = 7$ and 17 points, respectively. The next step would be to test the accuracy of the LAT transmission coefficients by the DILAT algorithm by finding the optimum number of M_S points that give the best compromise between accuracy and computational cost. The procedure to obtain the transmission coefficients was the one described in the previous section, i.e., a set of $\theta(\tilde{\alpha}_r, E_r)$ values at energies E_r, $r = 1, ..., M_S$ is chosen, with $E_{r=1}$ being the lowest tunneling energy at which it is possible to locate the classical turning points on the MEP for defining the straight path and $E_{r=M_S}$ being the last tunneling energy at which there is a nonadiabatic region along the straight path.

The deviation from the ILAT1D values of the DILAT transmission coefficients for different numbers of fitting points is given in Table 2 and plotted in Figure 3 for reactions R1−R4. For the present study, we have considered temperatures from 250 to 400 K, which for many practical applications is the temperature range for which one needs to evaluate the tunneling. At $T = 250$ K the smallest value of M_S that yields an accuracy better than 5% is $M_S = 13$ (and an interpolation with this value is hereafter called DILAT(13)). However, the interpolation using $M_S = 7$ (hereafter DILAT(7)), although it gives MUPES about three times larger than DILAT(13), yields small errors when

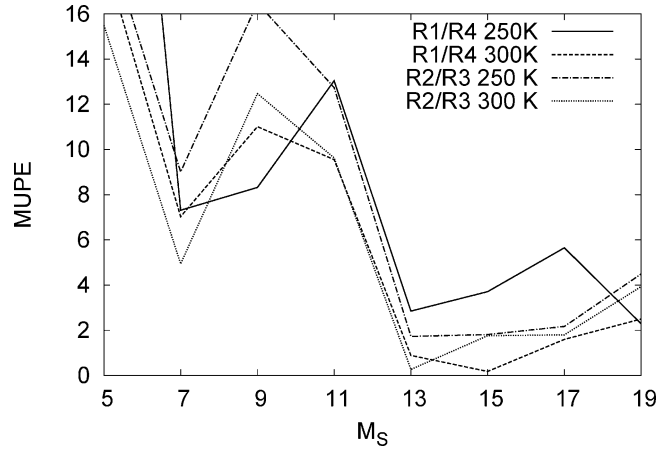

Figure 3. MUPEs for $\eta_{1,4}$ and $\eta_{2,3}$ KIEs obtained by the DILAT algorithm using different fitting points to a spline-undertension with respect to those LAT values obtained with the ILAT1D algorithm. The solid line plots the MUPE obtained at $T = 250$ and 300 K.

Table 3. Transmission Coefficients for Reactions R1−R4

			LCT[a]		LAT[b]		
reaction	T (K)	SCT	ILCT2D	μOMT[a]	DILAT(7)	DILAT(13)	ILAT1D
R1	250	21.9	28.1	31.4	39.4	36.1	36.3
	300	9.18	9.26	10.7	11.6	10.7	10.9
	350	5.32	4.97	5.78	5.75	5.43	5.52
	400	3.69	3.37	3.88	3.73	3.57	3.62
	500	2.37	2.16	2.42	2.28	2.22	2.25
R2	250	16.1	15.8	18.2	19.6	18.0	18.2
	300	7.40	6.83	7.91	7.79	7.27	7.39
	350	4.54	4.13	4.74	4.50	4.27	4.33
	400	3.27	2.98	3.36	3.16	3.03	3.07
	500	2.18	2.02	2.22	2.09	2.03	2.06
R3	250	15.2	10.7	16.0	11.8	11.7	12.1
	300	6.52	4.60	6.68	4.84	4.76	4.83
	350	3.94	2.92	3.98	3.00	2.98	2.99
	400	2.85	2.22	2.86	2.26	2.24	2.25
	500	1.95	1.64	1.95	1.66	1.65	1.65
R4	250	14.3	10.3	15.3	11.7	11.9	11.6
	300	6.29	4.49	6.47	4.65	4.68	4.70
	350	3.85	2.87	3.90	2.92	2.92	2.83
	400	2.80	2.20	2.82	2.22	2.22	2.22
	500	1.93	1.63	1.93	1.64	1.64	1.64

[a] From ref 71. There are errors in Table 7 of ref 71; the correct values of the LCT and μOMT transmission coefficients are listed here. [b] LAT transmission coefficients.

compared with $M_S = 9$ or 11 points and is about two times faster than DILAT(13), so comparisons involving both of them are interesting. At $T = 300$ K, all the MUPEs are smaller, with the largest errors for DILAT(7) and DILAT(13) being 6% and 1.7%, respectively. For reactions R1−R4, Table 3 shows the DILAT(7) and DILAT(13) transmission coefficients together with the reference ILAT1D transmission coefficients.

In general Table 2 shows convergence to about 5% and 1% at 250 and 300 K, respectively.

The transmission coefficients are compared in Table 3. To compute the KIEs $\eta_{1,4} \equiv k_{R1}/k_{R4}$ and $\eta_{2,3} \equiv k_{R2}/k_{R3}$ using several tunneling approximations, we have factored them into two contributions

$$\eta^{\mathrm{TST/X}} = \eta^{\mathrm{X}}_{\mathrm{tun}} \eta^{\mathrm{TST}} \tag{21}$$

Table 4. Calculated KIEs Using Various Approximations for Tunneling[a]

T (K)	η^{TST}	$\eta^{TST/SCT}$	$\eta^{TST/LCT}$	$\eta^{TST/\mu OMT}$	$\eta^{TST/LAT}$ [a]			η_{exp}[b]
				R1/R4				
250	7.8	11.9	21.3	16.0	26.3	23.7	24.4	–
300	5.8	8.4	11.9	9.6	14.5	13.3	13.5	–
350	4.6	6.4	8.0	6.8	9.1	8.6	9.0	–
400	3.9	5.1	6.0	5.4	6.5	6.3	6.4	6.5[c]
500	3.0	3.7	4.0	3.8	4.2	4.1	4.1	4.8[c]
				R2/R3				
250	5.7	6.0	8.4	6.5	9.4	8.8	8.6	–
300	4.4	5.0	6.5	5.2	7.1	6.7	6.7	–
350	3.7	4.3	5.3	4.4	5.7	5.3	5.4	13.0
400	3.2	3.6	4.3	3.2	4.5	4.3	4.4	8.5
500	2.6	2.9	3.2	3.0	3.3	3.2	3.2	5.0

[a] The last column lists the experimental KIEs. LAT transmission factors obtained with DILAT(7), DILAT(13), and ILAT1D algorithms are listed in columns 6−8, respectively. [b] From refs 80 and 81. [c] Erratum in Table 8 of ref 71; the correct values of the experimental KIEs are listed here.

In eq 21, η_{tun}^{X} includes quantum effects (tunneling plus nonclassical reflection) on the reaction coordinate using the approximation X, where X = SCT, LCT, μOMT, or LAT, and η^{TST} includes the symmetry numbers, the classical translational and rotational contributions, and the quasiclassical quantized vibrational contribution. (There is no potential energy contribution in the cases considered here because the variational transition state is the conventional transition state for these reactions.)

Table 4 lists the KIEs obtained by the different tunneling approximations together with the experimental[80,81] data. In general, all the methods underestimate the observed KIEs, although the ones obtained with the LAT approximation for tunneling are in better agreement with experimental values. The LCT transmission coefficients may underestimate the tunneling contribution in same cases, as was pointed out by Sansón et al.,[82] however the KIEs obtained by this approximation are quite similar to the LAT ones. The μOMT approximation gives similar results to those obtained with the LAT approximation for the hydrogen abstraction processes, but it gives larger values for the deuterium transfer. Therefore, this discrepancy is due to the magnitude of the SCT transmission coefficients for deuterium transfer, which has the effect of decreasing the calculated KIEs. In any case the $\eta_{2,3}$ KIEs calculated using the LAT approximation for tunneling are still too small when compared to the available experimental data. From these values we arrive to the same conclusions as in ref 71, i.e., at the moment we cannot explain this discrepancy, and we encourage further experiments on these systems.

Finally, it is interesting to analyze the errors (with respect to a ILAT1D calculation) of the DILAT method, not just in the case of the transmission coefficients but also in the context of the KIEs. In the worst scenario, the largest error in the evaluation of the KIEs would be the sum of the MUPEs, i.e., assuming no error cancellation. Using this worst-case possibility, we establish a maximum error of the DILAT(7) algorithm at $T = 250$ K of 9% for $\eta_{1,4}$ and $\eta_{2,3}$. For DILAT(13), these errors go down to 3% and 4% for $\eta_{1,4}$ and $\eta_{2,3}$, respectively. In round numbers, the errors of the DILAT(7) and DILAT(13) algorithms, at $T = 250$ K, are smaller than 10% and 5%, respectively. In fact the errors, as shown in Figure 3, due to error cancellation are 7% and 4% for $\eta_{1,4}$ and 9% and 2% for $\eta_{2,3}$ using DILAT(7) and DILAT(13), respectively.

At $T = 300$ K, if we assume no error cancellation, the MUPEs for $\eta_{1,4}$ and $\eta_{2,3}$ would be about 7% and 3% for DILAT(7) and DILAT(13), respectively. Similar calculated errors are obtained for DILAT(7), but when using DILAT(13), the calculated MUPEs are less than 1% for both of the two evaluated KIEs. These results are very encouraging, especially when we take into account that the DILAT(7) and DILAT(13) methods are, respectively, 6.6 and 3.6 times faster than ILAT1D and about 50 and 30 times faster than the full (uninterpolated) calculation. It should also be noticed that this is a difficult case with two or three minima in the action integral at every tunneling energy, so for reactions with a less abrupt PES, the errors are expected to be smaller. The present results show that the DILAT(13) algorithm is reliable above $T = 250$ K to within 5% for the cases studied, although more testing would be needed to make broadly applicable statements of this nature.

4. Concluding Remarks

We have presented two algorithms for efficient direct dynamics evaluation of the least-action tunneling (LAT) transmission coefficients for polyatomic reactions. The interpolated least-action tunneling method based on one-dimensional interpolation (ILAT1D) uses the same philosophy as the previous ILCT1D algorithm; in particular, both make use of spline-under-tension interpolations for the effective potentials in the nonadiabatic regions of the tunneling paths. This algorithm, depending on the system, is about 5−10 times faster than the full calculation without loss of accuracy. However, the ILAT1D procedure is still quite expensive for polyatomic systems, so we have developed a much less expensive algorithm called double interpolated least-action tunneling, DILAT, which employs one-dimensional interpolations of not only the effective potential along nonadiabatic portions of the tunneling paths but also of the values of the action integrals as functions of energy. This even simpler method still provides quite accurate results. The performance of the DILAT algorithm was tested for four hydrogen/deuterium abstraction reactions, and we found that the optimum number of effective potential energies to be calculated in the nonadiabatic region is $M_S = 13$. The DILAT method based on 13 tunneling energies can be from 3 to 5 times faster than the ILAT1D algorithm, depending on the characteristics of the nonadiabatic region, but with an error of less than 5%. The method is being incorporated into the POLYRATE computer program.

The LAT calculations do not account for the discrepancy from experimental $\eta_{2,3}$ KIEs of the previously computed KIEs that were based on the less accurate large-curvature

tunneling (LCT) approximation. This discrepancy remains unexplained.

Glossary

This glossary contains an explanation of all acronyms used in this article. The acronyms are explained at first use, but this is an extra guide for convenience.

CAG: classical adiabatic ground-state, a factor (usually close to unity) that makes the a transmission coefficient based on the vibrationally adiabatic ground-state potential curve consistent with a quasiclassical transition state calculation that implies a different threshold energy.

CVT: canonical variational theory, VTST applied to a canonical ensemble.

DILAT: doubly interpolated LAT.

ILAT1D: interpolated LAT method based on one-dimensional interpolation.

ILCT1D: interpolated LCT method based on one-dimensional interpolation.

ILCT2D: interpolated LCT method based on two-dimensional interpolation.

KIE: kinetic isotope effect, the ratio of rate constants for two reactions differing by isotopic substitution or isotopic placement.

LAG4: least action ground state, 4, version 4 of the LAT method when applied with the ground-state tunneling approximation.

LAT: least-action tunneling, a dynamical approximation for computing tunneling probabilities based on minimizing the magnitude of the imaginary part of the action integral along the tunneling path.

LCT: large-curvature tunneling, a dynamical approximation for computing tunneling probabilities that is appropriate when the MEP has large curvature in the tunneling region.

MEP: minimum-energy path in isoinertial coordinates.

μOMT: microcanonical OMT, a dynamical approximation for computing tunneling probabilities in which the choice between SCT and LCT tunneling is optimal at each tunneling energy (may be considered to be a poor person's version of LAT).

OMT: shorthand for μOMT.

PES: potential energy surface, same as potential energy function.

SCT: small-curvature tunneling, a dynamical approximation for computing tunneling probabilities that is appropriate when the MEP has only small curvature in the tunneling region.

VTST: variational transition-state theory, a theory for calculating absolute reaction rates from PES information.

VTST/MT: VTST with multidimensional tunneling, for example, with tunneling computed by the ZCT, SCT, LCT, μOMT, or LAT tunneling approximation.

ZCT: zero-curvature tunneling, a dynamical approximation for computing tunneling probabilities that assumes that the tunneling path is a straightened MEP and that the vibrational motions orthogonal to the tunneling path are adiabatic.

Acknowledgment. A. F.-R and R. M.-P. thank Xunta de Galicia for financial support through Axuda para a Consolidación e Estructuración de unidades de investigación competitivas do Sistema Universitario de Galicia, 2007/50, cofinanciada polo FEDER 2007−2013. This work was supported in part by the U.S. Department of Energy, Office of Basic Energy Sciences, under grant no. DE-FG02-86ER13579.

Supporting Information Available: The reactions used for the tests of the ILAT1D algorithm against full-LAT calculations. Number of single-point calculations (NSP) in the nonadiabatic region needed for the evaluation of the transmission coefficients by the full-LAT (taken as reference) and ILAT1D methods for reactions R5 to R9. Transmission coefficients, κ, evaluated at T = 200, 300, and 400 K by the full-LAT (taken as reference) and ILAT1D methods for reactions R5 to R9. This material is available free of charge via the Internet at http://pubs.acs.org.

References

(1) *Isotope Effects in Chemistry and Biology*; Kohen, A., Limbach, H. H., Eds.; CRC: Boca Raton, FL, 2006.

(2) *Hydrogen-Transfer Reactions*; Hynes, J. T., Schowen, R. L., Klinman, J. P., Limbach, H. H., Eds.; Wiley-VCH: Weinheim, Germany, 2007.

(3) Yamamoto, T. *J. Chem. Phys.* **1960**, *33*, 281.

(4) Kuppermann, A.; Greene, E. *J. Chem. Educ.* **1968**, *45*, 361.

(5) Manolopoulos, D. E.; Clary, D. C. *Annu. Rep. Prog. Chem., Sect. C: Phys. Chem.* **1989**, *86*, 95.

(6) Park, T. J.; Light, J. C. *J. Chem. Phys.* **1989**, *91*, 974.

(7) Truhlar, D. G.; Schwenke, D. W.; Kouri, D. J. *J. Phys. Chem.* **1990**, *94*, 7346.

(8) Gray, S. K.; Goldfield, E. M.; Schatz, G. C.; Balint-Kurti, G. G. *Phys. Chem. Chem. Phys.* **1999**, *1*, 1141.

(9) Mielke, S. L.; Lynch, G. C.; Truhlar, D. G.; Schwenke, D. W. *J. Phys. Chem.* **1994**, *98*, 8000.

(10) Bowman, J. M.; Wang, D.; Huang, X.; Huarte-Larrañaga, F.; Manthe, U. *J. Chem. Phys.* **2001**, *114*, 9683.

(11) Mielke, S. J.; Schwenke, D. W.; Garrett, B. C.; Truhlar, D. G.; Michael, J. V.; Su, M.-C.; W., S. J. *Phys. Rev. Lett.* **2003**, *91*, 63201.

(12) Balucani, N.; Skouteris, D.; Capozza, G.; Segoloni, E.; Casavecchia, P.; Alexander, M.; Capecchi, G.; Werner, H.-J. *Phys. Chem. Chem. Phys.* **2004**, *6*, 5007.

(13) Ceotto, C. S.; Yang, S.; Miller, W. H. *J. Chem. Phys.* **2005**, *122*, 044109.

(14) Chakraborty, A.; Truhlar, D. G. *Proc. Natl. Acad. Sci. U.S.A.* **2007**, *104*, 10774.

(15) Nyman, G.; van Harrevelt, R.; Manthe, U. *J. Phys. Chem. A* **2007**, *111*, 10331.

(16) Wentzel, G. *Z. Phys.* **1926**, *38*, 518.

(17) Kramers, H. A. *Z. Phys.* **1960**, *39*, 828.

(18) Brillouin, L. *Comptes Rendus* **1926**, *24*, 183.

(19) Kemble, E. C. *The Fundamental Principles of Quantum Mechanics with Elementary Applications*; Dover Publications: New York, 1937.

(20) Marcus, R. A.; Coltrin, M. E. *J. Chem. Phys.* **1977**, *67*, 2609.

(21) Garrett, B.; Truhlar, D. G.; Grev, R.; Magnuson, A. *J. Phys. Chem.* **1980**, *84*, 1730.

(22) Garrett, B. C.; Truhlar, D. G. *J. Chem. Phys.* **1983**, *79*, 4931.

(23) Garrett, B. C.; Abusalbi, N.; Kouri, D. J.; Truhlar, D. G. *J. Chem. Phys.* **1985**, *83*, 2252.

(24) Lynch, G. C.; Truhlar, D. G.; Garrett, B. C. *J. Chem. Phys.* **1989**, *90*, 3102.

(25) Taketsugu, T.; Hirao, K. *J. Chem. Phys.* **1997**, *107*, 10506.

(26) Tautermann, C. S.; Voegele, A. F.; Loerting, T.; Liedl, K. R. *J. Chem. Phys.* **2002**, *117*, 1962.

(27) Yamamoto, T.; Miller, W. H. *J. Chem. Phys.* **2003**, *118*, 2135.

(28) Meana-Pañeda, R.; Truhlar, D. G.; Fernández-Ramos, A. *J. Chem. Theory Comput.* **2010**, *6*, 6.

(29) Wigner, E. *J. Chem. Phys.* **1937**, *5*, 720.

(30) Horiuti, J. *Bull. Chem. Soc. Jpn.* **1938**, *13*, 210.

(31) Keck, J. C. *Adv. Chem. Phys.* **1967**, *13*, 85.

(32) Garrett, B. C.; Truhlar, D. G. *J. Chem. Phys.* **1979**, *70*, 1593.

(33) Garrett, B. C.; Truhlar, D. G. *Acc. Chem. Res.* **1980**, *13*, 440.

(34) Pechukas, P. *Annu. Rev. Phys. Chem.* **1981**, *32*, 159.

(35) Truhlar, D. G.; Hase, W. L.; Hynes, J. T. *J. Phys. Chem.* **1983**, *87*, 2664.

(36) Truhlar, D. G.; Garrett, B. C. *Annu. Rev. Phys. Chem.* **1984**, *35*, 159.

(37) Truhlar, D. G.; Isaacson, A. D.; Garrett, B. C. In *Theory of Chemical Reaction Dynamics*; Baer, M., Ed.; CRC: Boca Raton, FL, 1985; Vol. 4, p 65.

(38) Truhlar, D. G.; Garrett, B. C.; Klippenstein, S. J. *J. Phys. Chem.* **1996**, *100*, 12771.

(39) Garrett, B. C.; Truhlar, D. G. In *Theory and Applications of Computational Chemistry: The First Forty Years*; Dykstra, C. E.; Frenking, G., Kim, K. S., Scuseria, G. E., Eds.; CRC: Boca Raton, FL, 2005; p 67.

(40) Truhlar, D. G.; Garrett, B. C. In *Hydrogen-Transfer Reactions*; J. T. Hynes, H.-H. L.; Klinman, J. P., Schowen, R. L., Eds.; Wiley-VCH: Weinheim, Germany, 2007; Vol. 2, p 833.

(41) Fernández-Ramos, A.; Ellingson, A.; Garrett, B. C.; Truhlar, D. G. *Rev. Comput. Chem.* **2007**, *23*, 125.

(42) Allison, T. C.; Truhlar, D. G. In *Modern Methods for Multidimensional Dynamics Computations in Chemistry*; Thompson, D. L., Ed.; World Scientific: Singapore, 1998; p 618.

(43) Pu, J.; Gao, J.; Truhlar, D. G. *Chem. Rev.* **2006**, *106*, 3140.

(44) Eyring, H. *J. Chem. Phys.* **1935**, *3*, 107.

(45) Garrett, B. C.; Truhlar, D. G. *J. Chem. Phys.* **1980**, *72*, 3460.

(46) Garrett, B. C.; Truhlar, D. G.; Bowman, J. M.; Wagner, A. F.; Robie, D.; Arepalli, S.; Presser, N.; Gordon, R. J. *J. Am. Chem. Soc.* **1986**, *108*, 3515.

(47) Fernández-Ramos, A.; Smedarchina, Z.; Rodríguez-Otero, J. *J. Chem. Phys.* **2001**, *114*, 1567.

(48) Alhambra, C.; Sánchez, M. L.; Corchado, J. C.; Gao, J.; Truhlar, D. G. *Chem. Phys. Lett.* **2002**, *355*, 388.

(49) Nagel, Z.; Klinman, J. *Chem. Rev.* **2006**, *106*, 3095.

(50) Johnston, H. S. *Gas Phase Reaction Rate Theory*; Ronald Press: New York, 1966.

(51) Hirschfelder, J. O.; Wigner, E. *J. Chem. Phys.* **1939**, *7*, 616.

(52) Truhlar, D. G.; Kupperman, A. *J. Am. Chem. Soc.* **1971**, *93*, 1840.

(53) Kuppermann, A. *J. Phys. Chem.* **1979**, *83*, 171.

(54) Marcus, R. A. *J. Chem. Phys.* **1966**, *45*, 4493.

(55) Fukui, K.; Kato, S.; Fujimoto, H. *J. Am. Chem. Soc.* **1975**, *97*, 1.

(56) Truhlar, D. G.; Kuppermann, A. *J. Chem. Phys.* **1972**, *56*, 2232.

(57) Skodje, R. T.; Truhlar, D. G.; Garrett, B. C. *J. Phys. Chem.* **1981**, *85*, 3019.

(58) Skodje, R. T.; Truhlar, D. G.; Garrett, B. C. *J. Chem. Phys.* **1982**, *77*, 5955.

(59) Lu, D.-h.; Truong, T. N.; Melissas, V. S.; Lynch, G. C.; Liu, Y.-P.; Garrett, B. C.; Steckler, R.; Isaacson, A. D.; Rai, S. N.; Hancock, G. C.; Lauderdale, J. G.; Joseph, T.; Truhlar, D. G. *Comput. Phys. Commun.* **1992**, *71*, 235.

(60) Liu, Y.-P.; Lynch, G. C.; Truong, T. N.; Lu, D.-h.; Truhlar, D. G. *J. Am. Chem. Soc.* **1993**, *115*, 2408.

(61) Garrett, B. C.; Truhlar, D. G.; Wagner, A. F.; Dunning Jr, T. H. *J. Chem. Phys.* **1983**, *78*, 4400.

(62) Garrett, B. C.; Joseph, T.; Truong, T. N.; Truhlar, D. G. *Chem. Phys.* **1989**, *136*, 271.

(63) Truong, T. N.; Lu, D.-h.; Lynch, G. C.; Liu, Y.-P.; Melissas, V. S.; Stewart, J. J. P.; Steckler, R.; Garrett, B. C.; Isaacson, A. D.; González-Lafont, A.; Rai, S. N.; Hancock, G. C.; Joseph, T.; Truhlar, D. G. *Comput. Phys. Commun.* **1993**, *75*, 143.

(64) Liu, Y.-P.; Lu, D.-h.; González-Lafont, A.; Truhlar, D. G.; Garrett, B. C. *J. Am. Chem. Soc.* **1993**, *115*, 7806.

(65) Fernández-Ramos, A.; Truhlar, D. G. *J. Chem. Phys.* **2001**, *114*, 1491.

(66) Truhlar, D. G.; Brown, F. B.; Steckler, R.; Isaacson, A. D. In *The Theory of Chemical Reaction Dynamics*; Clary, D. C., Ed.; D. Reidel: Dordrecht, The Netherlands, 1986; p 285.

(67) Truhlar, D. G.; Gordon, M. S. *Science* **1990**, *249*, 491.

(68) González-Lafont, A.; Truong, T. N.; Truhlar, D. G. *J. Phys. Chem.* **1991**, *95*, 4618.

(69) *Quantum Tunneling in Enzyme-Catalysed Reactions*; Allemann, K., Scrutton, N. S., Eds.; RSC Publishing: Cambridge, UK, 2009.

(70) Renka, R. J.; Cline, A. K. *Rocky Mt. J. Math.* **1984**, *14*, 223.

(71) Fernández-Ramos, A.; Truhlar, D. G. *J. Chem. Theory Comput* **2005**, *1*, 1063.

(72) Fernández-Ramos, A.; Truhlar, D. G.; Corchado, J.; Espinosa-Garcia, J. *J. Phys. Chem. A* **2002**, *106*, 4957.

(73) Renka, R. J. *SIAM J. Sci. Stat. Comput.* **1987**, *8*, 393.

(74) Renka, R. J. *ACM Trans. Math. Software* **1993**, *19*, 81.

(75) Press, W. H.; Teukolsky, S. A.; Vetterling, W. T.; Flannery, B. P. *Numerical Recipies*, 3rd ed.; Cambridge University Press: Cambridge, UK, 2007; p 492.

(76) Truong, T. N.; Lu, D.-h.; Lynch, G. C.; Liu, Y.-P.; Melissas, V. S.; Stewart, J. J. P.; Steckler, R.; Garrett, B. C.; Isaacson, A. D.; González-Lafont, A.; Rai, S. N.; Hancock, G. C.; Joseph, T.; Truhlar, D. G. *Comput. Phys. Commun.* **1993**, *75*, 143.

(77) Zheng, J.; Zhang, S.; Lynch, B. J.; Corchado, J. C.; Chuang, Y.-Y.; Fast, P. L.; Hu, W.-P.; Liu, Y.-P.; Lynch, G. C.; Nguyen, K. A.; Jackels, C. F.; Fernández Ramos, A.; Ellingson, B. A.; Melissas, V. S.; Villa, J.; Rossi, I.; Coitiño, E. L.; Pu, J.; Albu, T. V.; Steckler, R.; Garrett, B. C.; Isaacson, A. D.; Truhlar, D. G. *POLYRATE*, 2008; University of Minnesota: Minneapolis, MN, 2008.

(78) Zhao, Y.; Lynch, B. J.; Truhlar, D. G. *J. Phys. Chem A* **2004**, *108*, 6908.

(79) Hehre, W. J.; Ditchfield, R.; Pople, J. A. *J. Chem. Phys.* **1972**, *56*, 2257.

(80) Sharp, T. E.; Johnston, H. S. *J. Chem. Phys.* **1962**, *37*, 1541.

(81) Carmichael, H.; Johnston, H. S. *J. Chem. Phys.* **1964**, *41*, 1975.

(82) Sansón, J. A.; Sánchez, M. L.; Corchado, J. *J. Phys. Chem. A* **2005**, *110*, 589.

CT100285A